Atmos. Meas. Tech. Discuss., 7, 6743–6790, 2014
www.atmos-meas-tech-discuss.net/7/6743/2014/
doi:10.5194/amtd-7-6743-2014

Atmospheric Measurement Techniques Discussions

Multi-station intercomparison of column-averaged methane from NDACC and TCCON: impact of dynamical variability

A. Ostler[1], R. Sussmann[1], M. Rettinger[1], N. M. Deutscher[3,4], S. Dohe[2], F. Hase[2], N. Jones[3], M. Palm[4], and B.-M. Sinnhuber[2]

[1]Karlsruhe Institute of Technology, IMK-IFU, Garmisch-Partenkirchen, Germany
[2]Karlsruhe Institute of Technology, IMK-ASF, Karlsruhe, Germany
[3]University of Wollongong, New South Wales, Australia
[4]Institute of Environmental Physics, University of Bremen, Germany

Received: 10 April 2014 – Accepted: 4 June 2014 – Published: 10 July 2014

Correspondence to: A. Ostler (andreas.ostler@kit.edu)

Published by Copernicus Publications on behalf of the European Geosciences Union.

Abstract

Dry-air column-averaged mole fractions of methane (XCH_4) retrieved from ground-based solar Fourier transform infrared (FTIR) measurements provide valuable information for satellite validation, evaluation of chemistry-transport models, and source-sink-inversions. In this context, Sussmann et al. (2013) have shown that mid-infrared (MIR) soundings from the Network for the Detection of Atmospheric Composition Change (NDACC) can be combined with near-infrared (NIR) soundings from the Total Carbon Column Observing Network (TCCON) without the need to apply an overall intercalibration factor. However, in spite of efforts to reduce a priori impact, some residual seasonal biases were identified, and the reasons behind remained unclear. In extension to this previous work, which was based on multi-annual quasi-coincident MIR and NIR measurements from the stations Garmisch (47.48° N, 11.06° E, 743 m a.s.l.) and Wollongong (34.41° S, 150.88° E, 30 m a.s.l.), we now investigate upgraded retrievals with longer temporal coverage and include three additional stations (Ny-Ålesund, 78.92° N, 11.93° E, 20 m a.s.l.; Karlsruhe, 49.08° N, 8.43° E, 110 m a.s.l.; Izaña, 28.31° N, 16.45° W, 2.370 m a.s.l.). Our intercomparison results (except for Ny-Ålesund) confirm that there is no overall bias between MIR and NIR XCH_4 retrievals, and all MIR and NIR time series reveal a quasi-periodic seasonal bias for all stations, except for Izaña.

We find that dynamical variability causes MIR–NIR differences of up to ~ 30 ppb for Ny-Ålesund, ~ 20 ppb for Wollongong, ~ 18 ppb for Garmisch, and ~ 12 ppb for Karlsruhe. The mechanisms behind this variability are elaborated via two case studies, one dealing with stratospheric subsidence induced by the polar vortex at Ny-Ålesund and the other with a deep stratospheric intrusion event at Garmisch. Smoothing effects caused by the dynamical variability during these events are different for MIR and NIR retrievals depending on the altitude of the perturbation area. MIR retrievals appear to be more realistic in the case of stratospheric subsidence, while NIR retrievals are more accurate in the case of stratosphere-troposphere exchange (STE) in the upper

AMTD
7, 6743–6790, 2014

troposphere/lower stratosphere (UTLS) region. About 35 % of the FTIR measurement days at Garmisch are impacted by STE, and about 23 % of the measurement days at Ny-Ålesund are influenced by polar vortex subsidence. The exclusion of data affected by these dynamical situations resulted in improved agreement of MIR and NIR seasonal cycles for Ny-Ålesund and Garmisch.

We found that dynamical variability is a key factor in constraining the accuracy of MIR and NIR seasonal cycles. The only way to avoid this problem is to use more realistic a priori profiles that take these dynamical events into account (e.g. via improved models), and/or to improve the FTIR retrievals to achieve a more uniform sensitivity at all altitudes (possibly including profile retrievals for the TCCON data).

1 Introduction

Atmospheric methane (CH_4) is the most important anthropogenic greenhouse gas after carbon dioxide. The radiative forcing (RF) from emissions of CH_4 for 2011 relative to the pre-industrial time (1750) is 0.97 W m^{-2} reflecting a significant contribution to the total anthropogenic RF of 2.29 W m^{-2} (Stocker et al., 2013). There is a diverse range of sources of CH_4 emissions from the Earth, coming from biogenic, thermogenic and pyrogenic formation processes. Among these three groups there are several sources that are driven by anthropogenic activities (livestock breeding, rice cultivation and, exploitation of fossil fuels), whereas other main sources of CH_4 are not directly influenced by humans (natural wetlands, bio mass burning, termites). However, there are large positive CH_4 feedbacks on climate warming such as increased emissions from wetlands and melting hydrates (Dlugokencky et al., 2011). The latter process has attracted special interest because a fast CH_4 release from the insulated hydrate reservoir would cause a massive warming effect within a few years (Archer, 2007).

Oxidation of atmospheric CH_4 by hydroxyl radicals (OH) is responsible for about 90 % of the global CH_4 sink. The remainder is absorbed by soils and by reactions with atomic and chlorine radicals in the stratosphere (Cicerone and Oremland, 1988).

AMTD
7, 6743–6790, 2014

Another minor oxidation sink is the reaction with chlorine radicals in the marine boundary layer (Allan et al., 2007).

As a consequence of an imbalance between CH_4 sources and sinks, the global CH_4 surface concentration has increased to ~ 1803 ppb in 2011, thereby exceeding the pre-industrial levels by about 150 % (Stocker et al., 2013). Attributing the changes of atmospheric CH_4 to source variations on historical time scales (Houweling et al., 2008; Sapart et al., 2012) as well as in the recent past (Bousquet et al., 2006, 2011; Kirschke et al., 2013) has been subject of extensive research, but is still associated with uncertainties. The ability to locate CH_4 emissions (anthropogenic and natural) on small spatial and temporal scales will be essential for future climate policy with regard to emission trading schemes. For this purpose, forward models and inversions need to be improved. As these rely strongly on CH_4 measurements, it is necessary to increase the network of CH_4 observations and to improve the accuracy of CH_4 measurements.

Indeed, the spatio-temporal coverage of atmospheric CH_4 measurements has been consistently improved since the early 1980s (Kirschke et al., 2013). Global networks for surface-based in situ measurements (i.e. Advanced Global Atmospheric Gases Experiment, AGAGE and network of National Oceanic and Atmospheric Administration, Earth System Research Laboratory, Global Monitoring Division, NOAA ESRL GMD) have been developed and airborne measurements in the free troposphere have been performed (e.g. Wofsy et al., 2011). Furthermore, remote-sensing measurements of CH_4 columns have been achieved by satellite instruments like SCIAMACHY (Scanning Imaging Absorption Spectrometer for Atmospheric Cartography) aboard ENVISAT (Environmental Satellite) and TANSO (Thermal And Near-infrared Sensor for carbon Observation) on GOSAT (Greenhouse Gases Observing Satellite). The ground-based equivalents of the satellite observations are represented by the high-precision Fourier-transform infrared (FTIR) measurements of the two established networks NDACC (Network for the Detection of Atmospheric Composition Change, http://www.ndacc.org/) and TCCON (Total Carbon Column Observing Network, http://www.tccon.caltech.edu/, Wunch et al., 2011), since both measure the same quantity as satellites.

AMTD
7, 6743–6790, 2014

Because of their high accuracy for column-integrated CH_4 measurements, both TCCON (Butz et al., 2011; Schneising et al., 2012; Yoshida et al., 2013; Fraser et al., 2013) and NDACC (Sussmann et al., 2005; De Mazière et al., 2008) data have been used for satellite validation. Satellite retrievals are used extensively in top-down estimates of CH_4 emissions (Bergamaschi et al., 2009, 2013; Fraser et al., 2013; Monteil et al., 2013; Houweling et al., 2013), therefore, NDACC/TCCON FTIR retrievals have a strong indirect influence on the accuracy of inversions. In addition, ground-based FTIR measurements can be directly utilized for validation of models (Houweling et al., 2010; Saito et al., 2012; Belikow et al., 2013) and inversions (Fraser et al., 2013). Thus, it is obvious that ground-based FTIR retrievals of column-averaged CH_4 are a cornerstone for satellite retrievals, chemistry transport models and inverse models.

By comparing column-averaged dry air mole fractions of methane (XCH_4) from NDACC and TCCON retrieved at the sites Garmisch (47.5° N) and Wollongong (34.5° S), Sussmann et al. (2013) showed that the data from both networks can be directly combined without performing an intercalibration. Because of its wider spatial and temporal coverage such a joint data set can provide major benefits for validation as well as for long-term trend analysis. However, the obtained agreement between NDACC and TCCON retrievals was not perfect despite applying a refined intercomparison strategy accounting for differing a priori profiles and averaging kernels. The reasons for these residual differences remained unexplained from this previous study.

In this paper we extend the previous work by Sussmann et al. (2013) by updating the FTIR time series and including three additional stations (Ny-Ålesund, 78.9° N, Karlsruhe, 49.1° N, and Izaña, 28.3° N), thereby covering diverse geophysical conditions. Besides the intercomparison of NDACC and TCCON measurements, the main focus of this study is understanding the impact of dynamical effects like stratospheric subsidence and stratosphere-troposphere exchange (STE) processes on the residual differences observed between NDACC and TCCON retrievals of CH_4.

Our paper is structured as follows: the participating FTIR sites and their measurement settings are introduced in Sect. 2 along with the MIR and NIR retrieval strategies.

AMTD
7, 6743–6790, 2014

After explaining the intercomparison strategy the corresponding results are shown in Sect. 3. Section 4 investigates in quantitative terms the impact of dynamical variability on residual differences between MIR and NIR retrievals. This is performed via analysis of one case study showing strong stratospheric subsidence induced by the polar vortex at Ny-Ålesund and another case study for a deep stratospheric intrusion event above Garmisch. Finally, Sect. 5 gives a summary and conclusions.

2 Ground-based soundings of columnar methane in the MIR and NIR

The NDACC infrared working group currently consists of 22 sites with measurements dating back up to two decades. The NDACC retrievals are obtained from solar absorption spectra recorded in the mid-infrared (MIR) spectral range. Since the establishment of TCCON in 2004, solar absorption measurements in the near-infrared (NIR) have started to provide high-precision retrievals of climate gases, like CO_2, CH_4, and N_2O (Wunch et al., 2011a). Today, there are around 20 operational TCCON sites.

The observational data set obtained from ground-based solar absorption measurements at Garmisch and Wollongong is extended by one year from the previous study of Sussmann et al. (2013), until the end of 2012. Additionally, the intercomparison data set is supplemented by FTIR measurements from three further sites (Ny-Ålesund, Karlsruhe, Izaña), thereby covering diverse geophysical conditions (Table 1). The solar FTIR systems of the individual sites are described in Appendix A. The intercomparison of MIR and NIR measurements requires that both MIR and NIR observations are performed in alternating mode.

For the analysis of NDACC- and TCCON-type measurements we used the spectral fitting software SFIT (or PROFFIT) and GFIT, respectively (Pougatchev et al., 1995; Hase et al., 2004; Wunch et al., 2011a). The MIR and NIR retrieval strategies are identical to the strategies used in Sussmann et al. (2013), with the exception of the update from GFIT ver. 4.4.10 to GFIT ver. 4.8.6 (GGG2012) which now includes the use of site- and time-dependent a priori profiles. The retrieval strategy MIR-GBM v1.1 (Sussmann

AMTD
7, 6743–6790, 2014

et al., 2011) is used for retrieving XCH_4 from measurements in the mid-infrared spectral region (2613–2921 cm^{-1}). Within SFIT (or PROFFIT) a full profile retrieval is set up using a Tikhonov-L1 regularization with an altitude-constant regularization strength. One fixed a priori volume mixing ratio (vmr) profile is used per site, derived from the Whole Atmosphere Chemistry Climate Model (WACCM, Garcia et al., 2007). The MIR XCH_4 is calculated by dividing the retrieved total column by the corresponding dry pressure column.

For the NIR retrievals GFIT uses an iterative method of scaling the a priori profile to provide the best fit to the measured spectrum in the near-infrared spectral region (5938–6076 cm^{-1}). The retrieved total column is divided by the dry pressure column derived from the simultaneously measured oxygen column (Wunch et al., 2011a) and subsequently scaled by the calibration factor 0.976. This calibration is used to account for spectroscopic uncertainties and was determined from various campaigns using coincident airborne in situ measurements calibrated to the WMO scale (Wunch et al., 2010; Geibel et al., 2012). In contrast to that, MIR retrievals are used without calibration.

Further details of the retrieval strategies can be found in Sussmann et al. (2013). Note that the MIR measurements of Karlsruhe and Izaña were analyzed with the retrieval code PROFFIT instead of SFIT. Differences in these retrieval codes are not expected to have an impact on the MIR retrievals as shown by Hase et al. (2004).

3 Intercomparison

3.1 Method

In addition to the direct intercomparison of MIR and NIR retrievals obtained with their individual retrieval a priori profiles, we will also investigate the intercomparison results after reducing the impact of differing a prioris of the MIR versus NIR retrievals. This achieved by the intercomparison strategy proposed by Sussmann et al. (2013),

AMTD
7, 6743–6790, 2014

see Eq. (1) therein. This strategy applies two crucial benefits: (i) Effects from differing a priori profiles are eliminated by an a posteriori adjustment of the soundings to a common a priori profile $\boldsymbol{x}_{\text{common}}$; (ii) differing smoothing terms caused by the differing averaging kernels are minimized by using time-dependent and site-dependent profiles $\boldsymbol{x}_{\text{common}}$ that are as close as possible to the true profile $\boldsymbol{x}_{\text{true}}$ at a site at the moment of observation. As in Sussmann et al. (2013) we use 3-hourly sampled CH_4 model profiles for $\boldsymbol{x}_{\text{common}}$. The model profiles are provided by the Center for Climate System Research/National Institute for Environmental Studies/Frontier Research Center for Global Change (CCSR/NIES/FRCGC) atmospheric general circulation model (AGCM) based CTM (hereafter, ACTM; Patra et al., 2009, 2011). The ACTM simulations are operated at T42 spectral truncation in the horizontal and 67 vertical levels reaching from the Earth's surface to the mesosphere (80 km). See Appendix B in Sussmann et al. (2013) for more details on the ACTM profiles.

Although the use of Eq. (1) in Sussmann et al. (2013) eliminates the impact of differing a priori profiles differences (MIR–NIR) can still arise because of a special smoothing effect as explained in the following. The smoothing term for the MIR retrieval is $(1 - \boldsymbol{a}^{l}_{\text{MIR}})(\boldsymbol{x}^{l}_{\text{common}} - \boldsymbol{x}^{l}_{\text{true}})$ where $\boldsymbol{a}^{l}_{\text{MIR}}$ is the total column averaging kernel of the MIR retrieval for model layer l. The analogous smoothing term for the NIR retrieval $(1 - \boldsymbol{a}^{l}_{\text{NIR}})(\boldsymbol{x}^{l}_{\text{common}} - \boldsymbol{x}^{l}_{\text{true}})$ is different because in general it holds that $\boldsymbol{a}^{l}_{\text{MIR}} \neq \boldsymbol{a}^{l}_{\text{NIR}}$. This aspect is crucial for understanding the origin of possible residual XCH_4 differences (NIR–MIR). The magnitude of such residual XCH_4 differences (MIR–NIR) depends on season because the averaging kernels show zenith angle dependence and, therefore, a seasonal behavior, shown in Fig. 2 in Sussmann et al. (2013). This seasonality of residuals will be discussed in Sect. 3.2 below. The differences are largest when the model differs the most from the true atmospheric profile, which is most likely to occur in special atmospheric situations. Examples for this can be cases with strong stratospheric subsidence or stratospheric intrusions. Case studies that illustrate this effect will be discussed in quantitative terms in Sect. 4.

AMTD
7, 6743–6790, 2014

The intercomparison is based on monthly means calculated from individual MIR and NIR measurements recorded on the same day. Only months with > 5 MIR and > 5 NIR measurements have been included.

3.2 Results

Figure 1a shows a scatter plot of the MIR and NIR monthly means containing data from all five FTIR sites as retrieved with their original retrieval a priori profiles. Error bars on data points are 2-σ uncertainties derived from the standard deviation (stdv) of the linear slope fit (2 stdv/$\sqrt{2}$) determined separately for each site, see Sussmann et al. (2013) for a discussion of this error characterization. The linear MIR/NIR slopes (obtained from linear fits forced through zero) are not significantly different from 1 for three stations, i.e. 1.0002(12) for Garmisch, 1.0010(13) for Wollongong and 0.9996(13) for Karlsruhe, see Table 2. However, they are significantly different from 1 for Izaña (0.9986(06)) and for Ny-Ålesund (0.9909(22)). The slope for Izaña corresponds to a small bias in XCH_4 (1.4 per mille) whereas there is a relatively big bias for Ny-Ålesund of 9.1 per mille. This means that the results of the direct intercomparison confirm the conclusion of Sussmann et al. (2013), that the MIR and NIR data set could be used together without the need of an intercalibration (except for Ny-Ålesund; possible reasons will be discussed in Sect. 4).

Figure 1b is the same as Fig. 1a but using ACTM profiles as common prior. The linear MIR/NIR slopes (obtained from linear fits forced through zero) are not significantly different from 1 for Garmisch (0.9994(09)) and Izaña (1.0007(07)). However, the MIR/NIR slopes are different from 1 for Karlsruhe (1.0024(11)), Wollongong (1.0030(11)), and Ny-Ålesund (0.9940(19)). It is not obvious that there is a significant improvement in the overall agreement of the MIR and NIR XCH_4 monthly means after the adjustment to the common prior, except at Ny-Ålesund, where the difference of the linear slope from 1 is reduced (from 0.9909(22) to 0.9940(19)) corresponding to a bias of 6 per mille. However, as explained in Sussmann et al. (2013) the main benefit of using the

AMTD
7, 6743–6790, 2014

common ACTM a priori is that the seasonalities of the MIR and NIR XCH_4 time series are in a better agreement.

The MIR and NIR monthly mean time series for all stations are shown in Fig. 2a–j, retrieved with both their original retrieval a prioris and with the common ACTM prior. It can be seen that for all stations except Izaña the stdv of the difference time series (Fig. 2a–j, upper trace) is reduced by using the ACTM profiles as common prior. For Izaña there is no reduction of the stdv (Fig. 2j) because the MIR and NIR time series are already in very good agreement (stdv = 2.5 ppb) without applying the a posteriori adjustment to a common a priori profile (Fig. 2i). This is probably due to generally favorable measurement conditions at Izaña with a high fraction of days with unperturbed clear sky conditions. An overview of all stdv's and MIR/NIR slopes is given in Table 2.

Although the use of ACTM as a common prior leads to an improved agreement between MIR and NIR XCH_4, there are still differences, which can reach levels up to 30 ppb for Ny-Ålesund (Fig. 2b), 20 ppb for Wollongong (Fig. 2d), 18 ppb for Garmisch (Fig. 2f), and 12 ppb for Karlsruhe (Fig. 2h). Furthermore, Fig. 2 shows a periodicity in the occurrence of the maximum differences at all stations except Izaña. These differences could potentially lead to biases in the inferred seasonal CH_4 flux patterns if used in model studies.

A principal explanation for such seasonal differences (MIR–NIR) has been given in Sect. 3.1, i.e. ACTM profiles cannot completely resolve the local dynamical variability caused by atmospheric processes like stratospheric subsidence or stratosphere-troposphere exchange processes. In order to investigate this effect in quantitative terms in the following section we present a case study of stratospheric subsidence induced by the polar vortex at Ny-Ålesund and another case study of a deep stratospheric intrusion event at Garmisch.

AMTD
7, 6743–6790, 2014

4 Effects of dynamical variability

4.1 Impact of subsidence

The motivation of this case study is to demonstrate and explain the effects of polar subsidence on the MIR and NIR retrievals (Sect. 4.1.1). Furthermore, the total impact on the intercalibration results for Ny-Ålesund is inferred by excluding FTIR measurements that are affected by polar vortex subsidence (Sect. 4.1.2).

4.1.1 Case study I: Ny-Ålesund on 25 March 2011

As shown by Lindenmaier et al. (2012) and Sinnhuber et al. (2011) the meteorological conditions during winter/spring 2011 formed a strong polar vortex that persisted into April. Besides that, high potential vorticity (PV) values of 46 PVU (potential vorticity unit) on the 450 K potential temperature (PT) surface (ECMWF re-analysis, European Centre for Medium-Range Weather Forecasts) strongly indicate that Ny-Ålesund was underneath the area of the polar vortex on 25 March 2011.

Therefore, we investigate the impact of replacing the ACTM-based a priori profile with a strongly subsided CH_4 profile, which is typical for intra-vortex conditions and may be more realistic for 25 March 2011 above Ny-Ålesund. Such a profile (labeled MIR a priori$_{subsided}$) is given in Fig. 3a along with the ACTM profile for 25 March 2011 and the standard retrieval a prioris. This subsided profile corresponds to the MIR standard retrieval a priori from WACCM, which has been modified to account for subsidence according to Toon et al. (1992), see Appendix B for details.

Figure 4 shows the MIR and NIR XCH_4 as computed using the original ACTM as common prior along with the case using MIR a priori$_{subsided}$. It can be seen that in the case of using the original ACTM as a common prior, there is a significant difference between the NIR and MIR retrievals ($\sim$ 29 ppb for the time period 08:00–10:00 UT), while there is good agreement if using the subsided profile MIR a priori$_{subsided}$ (mean difference of $\sim$ 6 ppb for the time period 08:00–10:00 UT). Most of the difference arises

AMTD
7, 6743–6790, 2014

from the fact that the NIR data based on ACTM prior are reduced by ∼ 31 ppb (for the time interval 08:00–10:00 UT) if MIR a priori$_{subsided}$ is used instead. For the MIR data the reduction due to the use of MIR a priori$_{subsided}$ is only ∼ 8 ppb. This is due to the fact that the NIR total column kernels are not as sensitive as the MIR total column kernels in the lower stratosphere (see Fig. 3b). Figure C1 shows an analogous plot with the MIR and NIR retrievals based on their original standard a prioris. The effect of using the subsided profile (MIR a priori$_{subsided}$) instead of the original standard retrieval a prioris is very similar to the effect described with regard to Fig. 4, i.e. the difference between the NIR and MIR retrievals is reduced from ∼ 37 ppb to ∼ 6 ppb (for the time period 08:00–10:00 UT). Furthermore, MIR and NIR retrievals are reduced by 4 and 35 ppb, respectively, compared to the standard a prioris.

Our case study for Ny-Ålesund shows in quantitative terms that the effect of polar subsidence on ($\boldsymbol{x}'_{common} - \boldsymbol{x}'_{true}$) can be high enough to significantly impact the accuracy of the MIR and NIR retrievals in a different way. Especially the NIR retrievals are significantly affected when using a priori profiles which do not account for stratospheric subsidence, because their averaging kernels are less sensitive in the stratosphere.

4.1.2 Exclusion of subsidence events

While the case study in Sect. 4.1.1 was focused on the different impacts of stratospheric subsidence on the MIR and NIR retrievals for a single day, we now investigate the overall impact of subsidence on the full Ny-Ålesund time series used for the intercomparison of MIR and NIR XCH_4 retrievals.

To identify the location of the polar vortex and the onset and breakup dates of the vortex, we used the criteria from Nash et al. (1996). Thereby, we determined if Ny-Ålesund was inside the vortex or not at the 450 K potential temperature level (about 18 km altitude). Figure 5 shows the number of FTIR measurement days at Ny-Ålesund that were influenced by the polar vortex together with the total number of FTIR measurement days, separated by year. As FTIR measurements (MIR and NIR) at Ny-Ålesund are typically performed from the middle of March until end of September, the overlap time

AMTD
7, 6743–6790, 2014

with the polar vortex period is limited to early spring. We found that the relative fraction of FTIR measurement days influenced by the polar vortex is ∼ 63 % in March and ∼ 57 % in April (averaged for the time period 2005–2012).

FTIR measurement days influenced by the polar vortex were excluded from the MIR/NIR intercomparison and monthly mean scatter plots (MIR versus NIR) were analyzed via linear fits. The parameters from these fits are listed in Table 3. The linear MIR/NIR slope of the data set that is corrected to ACTM as common prior is improved from 0.9940(19) to 0.9950(20) and the stdv is further reduced from 11.5 ppb to 11.0 ppb.

Despite these positive effects of the exclusion of polar vortex situations on the overall intercomparison, there are still significant residual XCH_4 differences (MIR–NIR) for Ny-Ålesund, which vary temporally (see Fig. C2). Hence, we speculate that deviations of the ACTM profiles from the true profiles in the stratosphere also occur outside the early spring period. Indeed, besides subsidence, there are further dynamical processes in the UTLS region that may contribute to a variability of the CH_4 profile not captured by ACTM. This assumption is supported by the fact that the residual XCH_4 differences from the stations Garmisch, Wollongong, and Karlsruhe cannot be linked to the polar vortex subsidence because of their geographical position. Therefore, the emphasis of Sect. 4.2 lies on the impact of dynamical variability caused by stratosphere-troposphere exchange (STE) processes.

4.2 Impact of stratosphere-troposphere exchange processes

Stratosphere-troposphere exchange (STE) processes cause the transport of air-masses across the tropopause. For a detailed overview of the extensive research related to STE processes with some focus on processes in the extra tropics we refer to Stohl et al. (2003). A considerable part of STE research dealt with the impacts of STE on the tropospheric ozone (O_3) budget due to its relevance to air quality (Stohl and Trickl, 1999; Stohl et al., 2000; Trickl et al., 2003, 2010). Recently, by using a high-resolution chemistry transport model Lin et al. (2012) were able to show that

AMTD
7, 6743–6790, 2014

stratospheric intrusions in springtime of 2010 significantly increased surface ozone at high-elevation western US sites.

Whereas ozone related STE processes have been well studied, the impact of STE processes on the CH_4 budget has not been investigated very much. Nevertheless, by observing a stratospheric intrusion event on 27 March 2010, Xiong et al. (2013) revealed that areas with depleted CH_4 are collocated with enhanced O_3. They analyzed data from Atmospheric Infrared Sounder (AIRS) retrievals and used aircraft in situ measurements that confirmed that CH_4 depletion occurred down to 550 hPa with a decrease in mixing ratios of up to 100 ppb.

In order to investigate the (possibly differing) impact of STE processes on MIR and NIR retrievals of XCH_4, Sect. 4.2.1 deals with a stratospheric intrusion event on 6 March 2008 at Garmisch. After that, the aim of Sect. 4.2.2 is to estimate the percentage of FTIR measurements that are affected by STE-processes, and to identify the consequences for the intercomparison of MIR and NIR retrievals at Garmisch.

4.2.1 Case study II: Garmisch on 6 March 2008

Figure 6a shows the single MIR and NIR XCH_4 values on 6 March 2008 as computed with the a posteriori adjustment to the common ACTM prior. It is obvious that the agreement between MIR and NIR XCH_4 is very good until 11:00 UTC, but then the NIR XCH_4 increases by about 25 ppb within one hour. In contrast to that the MIR XCH_4 increases only slightly, and this results in high XCH_4 residuals (NIR–MIR $\sim$ 15 ppb).

We will show in the following that this significant increase in XCH_4 differences within a short time scale of one hour is caused by a deep stratospheric intrusion event that was observed by the tropospheric ozone lidar at Garmisch. Details and illustrations of lidar sounding series detecting stratospheric intrusions very similar to our 6 March 2008 case can be found e.g. in Trickl et al. (2010). The lidar sounding series of 6 March 2008 (to be published by Trickl et al., 2014) points to the occurrence of various layers with elevated ozone levels generated by a stratospheric intrusion. Until 11:00 UTC, there is one layer existing approximately in the altitude range 2–4 km and a second layer in the

AMTD
7, 6743–6790, 2014

range 6–10 km. Both regions are characterized by enhanced O_3 volume mixing ratios (typically up to 125 ppb). These layers with elevated ozone concentrations correspond to areas of depleted CH_4 volume mixing ratios. According to the lidar sounding, after 11:00 UTC there remains only one layer with ozone rich air masses, i.e. CH_4-depleted air masses in the UTLS region (8–15 km).

To respond to the dynamical variability induced by the stratospheric intrusion the MIR and NIR retrievals were re-corrected (Fig. 6b). The ACTM profiles were modified in a simple manner to represent the depletion of CH_4 before 11:00 UTC ($ACTM_{intrusion1}$) and after 11:00 UTC ($ACTM_{intrusion2}$). The magnitudes of the CH_4 depletions used in Fig. 7a correspond to typical values reported in the study by Xiong et al. (2013).

The transformation of O_3 lidar soundings into CH_4 profiles is just a semi-quantitative approach. However, the re-correction of the MIR and NIR retrievals to the modified ACTM a priori profiles of Fig. 7a results in a nearly perfect agreement between MIR and NIR XCH_4 as shown in Fig. 6b. The re-correction effect on the NIR retrievals is small (< 5 ppb) because the NIR total column retrievals shows high sensitivity in the troposphere and the lowest stratosphere (see Fig. 7b). The effect on the MIR retrievals, however, is twofold: although the MIR total column kernels are not perfectly sensitive in the troposphere (Fig. 7b) there is almost no re-correction effect on the MIR retrievals until 11:00 UTC. This is because of two smoothing effects, which compensated each other before the re-correction was applied. The lower-layer CH_4 depletion (Fig. 7a, $ACTM_{intrusion1}$, 2–4 km) was underestimated (see MIR averaging kernel in Fig. 7b) while the upper-layer CH_4 depletion (Fig. 7a, $ACTM_{intrusion1}$, 6–10 km) was overestimated (see MIR averaging kernel in Fig. 7b). Therefore, there was no net effect on the MIR retrievals before 11:00 UTC. However, after 11:00 UTC, MIR XCH_4 was significantly lower than NIR XCH_4 because of an overestimation of the CH_4 depletion in the UTLS region (Fig. 7a, $ACTM_{intrusion2}$, 8–15 km, see MIR averaging kernel in Fig. 7b). The re-correction effect on MIR retrievals after 11:00 UTC corresponds to an increase in XCH_4 of up to 15 ppb. Alltogether, we are able to explain the diurnal variation of

AMTD
7, 6743–6790, 2014

the re-corrected MIR and NIR XCH_4 (Fig. 6b) in relation to the basic features of the stratospheric intrusion above Garmisch.

Finally, we can understand the significant step in both MIR and NIR XCH_4 which can be seen after 11:00 UTC. The two tropospheric layers of CH_4-depleted air in the time period until their dissipation at 11:00 UTC have a bigger impact on XCH_4 compared to the CH_4 depletion in the UTLS after 11:00 UTC because the relative fraction of air mass is higher in the troposphere. Therefore, the mean XCH_4 (NIR, MIR) before 11:00 UTC is about 20 ppb lower than for the time period after 11:00 UTC. This is the first time that such a significant intra-day increase in XCH_4 (1.15 %) could be detected from ground-based FTIR retrievals and explained by the dynamical variability of a stratospheric intrusion event.

4.2.2 Exclusion of STE-events

For the detection of stratospheric intrusions coincident to FTIR measurements at Garmisch we adapted an approach for the analysis of stratospheric intrusions that was introduced by Trickl et al. (2010). This strategy uses STE trajectories based on ECMWF data. These STE trajectories represent a small subset of four-day forward trajectories calculated with the Lagrangian Analysis Tool (LAGRANTO; Wernli and Davies, 1997) and are defined through two requirements: they are (i) initially residing in the stratosphere and then (ii) during the following four days are descending by more than 300 hPa into the troposphere.

For each day, STE trajectories have been calculated for the start times 00:00 UTC and 12:00 UTC, and distributed by automated electronic mail by ETH Zürich (Swiss Federal Institute of Technology). As an example, Fig. 8 shows the intrusion trajectories initiated on 16 August 2007 at 12:00 UTC. For the identification of the stratospheric intrusions at Garmisch we defined a detection area of $\pm 1^{\circ}$ (latitude and longitude) around Garmisch (see Fig. 8 blue square). As a further requirement for counting a stratospheric intrusion, at least 5 trajectories should touch or hit the detection area.

AMTD
7, 6743–6790, 2014

In addition, trajectory calculations were carried out with the HYSPLIT model. The HYSPLIT trajectories were evaluated according to the approach by Trickl et al. (2010, Sect. 2.3 therein) for identifying stratospheric intrusions at Garmisch. (Note that the detection analysis of stratospheric intrusions could not be made for the complete FTIR data set because of some missing trajectories. Nevertheless, the analysis covers the majority of the FTIR measurements.)

Our analysis reveals that ∼ 35 % of the FTIR measurement days at Garmisch are influenced by STE processes. The exclusion of the affected XCH_4 data yields a significantly improved agreement between MIR and NIR retrievals as retrieved with their original retrieval a priori profiles. The same holds true using ACTM as common prior, see Fig. 9a and b, respectively. The stdv of the difference time series NIR–MIR using the original and common ACTM priors (see Fig. C3) is reduced from 8.2 ppb to 6.5 ppb and from 6.2 ppb to 4.7 ppb, respectively. All fit parameters for the data sets of the STE analysis at Garmisch are given in Table 4.

The improved agreement is achieved by the fact that measurement days with high residual XCH_4 differences, caused by different smoothing terms related to STE, are filtered out. Winter months are particularly affected by this extra filter criterion. This is in accordance with Sprenger and Wernli (2003), who showed that STE in the Northern Hemisphere has a distinct seasonal cycle with a flat maximum from December to April and a pronounced minimum in August and September.

Another outcome from Sprenger and Wernli (2003) is that at a subtropical site like Izaña the frequency of STE events is much lower than at mid-latitude sites like Garmisch, Karlsruhe, or Wollongong. Hence, the overall impact of STE processes on Izaña MIR and NIR retrievals is small compared to the other sites. This is confirmed by the very good agreement between MIR and NIR seasonalities at Izaña. Also, the polar site Ny-Ålesund is more influenced by STE processes than Izaña and thereby the MIR and NIR retrievals at Ny-Ålesund are affected by a second mechanism of dynamical variability in addition to polar subsidence. Besides that, we expect that remaining XCH_4 differences (NIR–MIR) are caused by near-surface CH_4 variations in combination with

AMTD
7, 6743–6790, 2014

different MIR and NIR retrieval sensitivities. As the high mountain site Izaña is usually located above the planetary boundary layer (PBL), there should not be an impact on MIR and NIR retrievals. In contrast to that, Garmisch is located inside the PBL and therefore MIR and NIR retrievals are affected by this CH_4 variability. For this reason, MIR and NIR retrievals at Izaña are expected to be in better agreement compared to Garmisch (and this is in line with our results), although retrievals affected by STE processes have been excluded for Garmisch.

Finally, the qualitative findings from the STE analysis of MIR and NIR retrievals at Garmisch can be transferred directly to the sites Karlsruhe, Wollongong, and Ny-Ålesund. As explained above, they are consistent with the site-specific characteristics at Izaña.

5 Summary and conclusions

We have compared MIR (NDACC) and NIR (TCCON) retrievals of XCH_4 obtained at the sites Garmisch, Karlsruhe, Izaña, Wollongong, and Ny-Ålesund. Our intercomparison results (Table 2) confirm the major findings from Sussmann et al. (2013). That is, there is no need to apply an MIR/NIR intercalibration factor due to very good overall agreement of the original MIR and NIR data sets as retrieved (except Ny-Ålesund). Furthermore, we showed that the remaining seasonal bias could be reduced by using a realistic site-specific and time-dependent common prior (ACTM). However, residual differences in Sussmann et al. (2013) and also in the present study reached significant levels (up to ~ 30 ppb for Ny-Ålesund), limiting the accuracy of the MIR and NIR seasonal cycles.

In this paper we were able to show that dynamical variability is the main source for these residual differences. Thereby, we complement the outcomes from Sussmann et al. (2013) with important additional findings about the characteristics of MIR and NIR retrievals of methane.

AMTD
7, 6743–6790, 2014

In extreme scenarios of atmospheric variability, i.e. stratospheric subsidence or deep STE-events, the approach using a common model prior to reduce differing smoothing errors fails because the model profile is likely to deviate from the true atmospheric CH_4 profile. By means of a case study we showed that stratospheric subsidence at Ny-Ålesund is associated with large differences between MIR and NIR retrievals (~ 29 ppb for the time period 08:00–10:00 UT on 25 March 2011). Another case study indicated that a deep stratospheric intrusion at Garmisch gives rise to residual differences of up to ~ 15 ppb. Due to the different vertical sensitivities (averaging kernels), the smoothing effects of MIR and NIR retrievals are unequal for both case studies. While NIR retrievals are affected by stratospheric subsidence more than MIR retrievals, the situation is reversed for STE-processes like deep stratospheric intrusions. As a consequence, both the exclusion of Ny-Ålesund retrievals affected by stratospheric subsidence and the exclusion of Garmisch retrievals affected by STE-processes resulted in improved agreement of MIR and NIR seasonal cycles (Tables 3 and 4).

We found that 23 % of the FTIR measurement days at Ny-Ålesund are influenced by the polar vortex and 35 % of the FTIR measurement days at Garmisch are influenced by STE. Considering that the high increase in XCH_4 of ~ 25 ppb within one hour at Garmisch is related to a deep stratospheric intrusion, it is obvious that such STE-processes are able to introduce a remarkable variation in XCH_4. From the geographical and seasonal variability of STE presented in Sprenger and Wernli (2003) we conclude that, in contrast to Izaña, the other mid-latitude sites (Karlsruhe, Wollongong) and the polar site (Ny-Ålesund) are also affected by STE-processes. This is in line with the very good agreement of the MIR and NIR seasonal cycles for Izaña.

We conclude that atmospheric variability is a key factor in constraining the accuracy of MIR and NIR seasonal cycles. The quality of MIR and NIR data is directly linked to smoothing effects. Therefore, NIR retrievals at polar sites may be improved by accounting for stratospheric subsidence in the standard retrieval a priori. Improving the quality of MIR retrievals affected by STE seems to be more complicated due to the diversity of STE-processes. However, we conjecture that more realistic a priori profiles

AMTD
7, 6743–6790, 2014

from high-resolution models reflecting small-scale processes could help to reduce MIR smoothing effects. An alternative method to overcome this problem would be to further improve the FTIR retrievals with the target to achieve a more uniform sensitivity at all altitudes. i.e., if the MIR averaging kernel was more evenly weighted with altitude then the MIR dependence on STE should be reduced. Also, using a formal optimal estimation (OE) inverse technique in GFIT could foreseeably help to improve the sensitivity of NIR retrievals to subsidence.

Besides that, the outcomes of this paper confirm that the inclusion of an accurate model representation of atmospheric transport is essential for inverse models when using MIR and NIR retrievals of XCH_4. For instance, within inverse models MIR and NIR XCH_4 variations from dynamical variability will be attributed incorrectly to distributions and magnitudes of CH_4 emissions if the atmospheric transport model is not precise.

When using NDACC and/or TCCON XCH_4 data, it is critical to be aware of the effects of dynamical events on the accuracy of the relevant data set. Depending on the requirements on data accuracy, NDACC and/or TCCON XCH_4 data can be used with or without the exclusion of dynamical events. Methods to detect these events have been presented in this study. Given a proper data use based on the findings in this paper, a joint NDACC and TCCON data set will result in wider spatial and longer temporal coverage of XCH_4 data for the validation of top-down estimates, satellite validation, and trend studies.

Appendix A: Description of FTIR sounding sites

A1 Garmisch

The Garmisch solar FTIR system (47.48° N, 11.06° E, 743 m a.s.l.) is operated by the group "Variability and Trends" at the Institute of Meteorology and Climate Research – Atmospheric Environmental Research (IMK-IFU), Karlsruhe Institute of Technology (KIT). Column-averaged methane is retrieved from FTIR measurements performed with

AMTD
7, 6743–6790, 2014

a Bruker IFS125HR interferometer. NIR forward and backward single-scan measurements are recorded with an InGaAs detector by using a maximum optical path difference of 45 cm. In the MIR spectral range the solar absorption spectra are detected with an InSb detector using a maximum optical path difference of 175 cm and averaging six scans with an integration time of approximately seven minutes.

The Garmisch FTIR system took part in the aircraft calibration campaign of the EU project IMECC (Infrastructure for Measurement of the European Carbon Cycle) (Messerschmidt et al., 2011; Geibel et al., 2012). Garmisch FTIR measurements have been used for satellite validation (de Laat et al., 2010; Morino et al., 2011; Wunch et al., 2011b), carbon cycle research (Chevallier et al., 2011), and studies of atmospheric variability and trends (e.g., Borsdorff and Sussmann, 2009; Sussmann et al., 2009, 2012). The intercalibration of MIR and NIR measurements in this study covers the time period from July 2007–December 2012.

A2 Wollongong

The Wollongong solar FTIR system (34.41° S, 150.88° E, 30 m a.s.l.) is operated by the Center for Atmospheric Chemistry at the University of Wollongong, Australia. The intercomparison uses the Wollongong time series of June 2008–December 2012. In this time period the FTIR measurements were performed with a Bruker IFS125HR instrument. The settings for NIR measurements are identical to those at Garmisch. In the MIR spectral range solar absorption spectra were recorded with an InSb detector, using an optical path difference of 257 cm and averaging two scans with an integration time of approximately four minutes. Data obtained from Wollongong FTIR have contributed to a chemistry-transport model validation by using MIR measurements of stratospheric tracer total column abundances (Kohlhepp et al., 2012).

AMTD
7, 6743–6790, 2014

A3 Karlsruhe

The Karlsruhe solar FTIR system (49.08° N, 8.43° E, 110 m a.s.l.) is operated by the group "Ground-based remote-sensing" at the Institute for Meteorology and Climate Research – Atmospheric Trace Gases (IMK-ASF), KIT, Germany. In 2009 a new FTIR container with a Bruker IFS125HR interferometer has been set up for solar absorption measurements in the MIR and NIR.

The settings for NIR measurements are identical to those at Garmisch. MIR measurements are performed with an InSb detector using a maximum optical path difference of 180 cm. Four scans are averaged with an integration time of 9.5 min. This study uses MIR and NIR measurements out of the time period from March 2010–December 2012. The Karlsruhe FTIR system participated in the aircraft calibration campaign of the EU project IMECC.

A4 Izaña

The Izaña solar FTIR system (28.31° N, 16.45° W, 2370 m a.s.l.) is located on the Canary Island of Tenerife and is part of a collaboration between the Meteorological State Agency of Spain (Spanish acronym: AEMET) and KIT. It is operated by the Izaña Atmospheric Research Center and the responsibility for the FTIR experiment lies with IMK-ASF of the Karlsruhe Institute for Technology (KIT).

Because measurements from 2007–2010 are affected by laser sampling ghosts the intercalibration only uses FTIR data from December 2010–December 2012 which have been recorded with a Bruker IFS125HR interferometer. The settings for NIR measurements are identical to those at Karlsruhe. The interferograms for the MIR retrievals are operated with an InSb detector using a maximum optical path difference of 180 cm before averaging six scans with an integration time of about seven minutes. Izaña FTIR measurements have been used for a long-term validation of tropospheric column-averaged methane in the mid- infrared spectral region (Sepulveda et al., 2012) and

AMTD
7, 6743–6790, 2014

have also been part of technical study about a method for ghost correction in historic near-infrared FTIR measurements (Dohe et al., 2013).

A5 Ny-Ålesund

The Ny-Ålesund solar FTIR system (78.92° N, 11.93° E, 20 m a.s.l.) is part of the the joint French-German Polar Research Base AWIPEV (Alfred Wegener Institute for Polar and Marine Research and the French Polar Institute Paul Emile Victor) on the Svalbard archipelago. The intercalibration contains FTIR measurements from March 2005–August 2012 which have been performed with a Bruker 120HR interferometer by the AWI Potsdam and the University of Bremen. Ground-based solar absorption measurements are operated from the end of March until the end of September when the polar night begins.

Column-averaged methane is retrieved from double-scan TCCON-type measurements recorded with an InGaAs diode using a maximum optical path difference of 30 cm. No DC/solar intensity variation correction was applied to Ny-Ålesund data. MIR retrievals are recorded with an InSb detector by using an optical path difference of 180 cm. Two scans are averaged with an integration time of approximately 2.5 min.

Appendix B: Derivation of a typical strongly subsided CH_4 profile for Ny-Ålesund

Inside the polar vortex stratospheric subsidence leads to a depletion of the total columns of tropospheric source gases, whereas outside the polar vortex the columns of these gases remain unchanged. Based on the assumption that this variation of total columns is the result of vertical transport alone, Toon et al. (1992) derived a mapping transformation which links points on the vmr profile outside the vortex to the same vmr inside according to the relation

$$\mathrm{vmr}_{\mathrm{subsided}}(z) = \mathrm{vmr}(z(1 + \mathrm{DOS})), \tag{B1}$$

where DOS is the degree of subsidence.

AMTD
7, 6743–6790, 2014

As explained in Sect. 4.1.1 Ny-Ålesund was affected by strong subsidence on 25 March 2011. Therefore, we decided to use a typical maximum DOS value of 0.44 to account for subsidence in the MIR and NIR retrievals on 25 March 2011. Equation (B1) was applied to the MIR original a priori profile (from WACCM) above the tropopause to get a subsided common prior (see Fig. 3a, MIR a priori$_{\text{subsided}}$).

Acknowledgements. We are indebted to P. K. Patra (JAMSTEC) for providing ACTM model data and thank T. Blumenstock (KIT) and O. E. García-Rodríguez (AEMET) for making Izaña FTIR data available. Furthermore, we thank D.W.T. Griffith (University of Wollongong) and J. Notholt (IUP) for providing FTIR data from Wollongong and Ny-Ålesund, respectively. We thank H. P. Schmid (IMK-IFU) for his continual interest in this work. Provision of the GFIT code by G. Toon (JPL) is gratefully acknowledged. Our work has been performed as part of the ESA GHG-cci project via subcontract with the University of Bremen. In addition we acknowledge funding by the EC within the INGOS project. We thank the ECMWF for providing access to the meteorological data. We thank for support by the Deutsche Forschungsgemeinschaft and Open Access Publishing Fund of the Karlsruhe Institute of Technology. The Wollongong work was funded through the Australian International Science Linkage grant CG130014 and the Australian Research Council, grants DP0879468 and DP110103118.

The service charges for this open access publication have been covered by a Research Centre of the Helmholtz Association.

References

Allan, W., Struthers, H., and Lowe, D. C.: Methane carbon isotope effects caused by atomic chlorine in the marine boundary layer: global model results compared with Southern Hemisphere measurements, J. Geophys. Res., 112, D04306, doi:10.1029/2006JD007369, 2007.

Archer, D.: Methane hydrate stability and anthropogenic climate change, Global Biogeochem. Cy., 4, 521–544, doi:10.5194/bg-4-521-2007, 2007.

AMTD

7, 6743–6790, 2014

Belikov, D., Maksyutov, S., Miyasaka, T., Saeki, T., Zhuravlev, R., and Kiryushov, B.: Mass-conserving tracer transport modelling on a reduced latitude-longitude grid with NIES-TM, Geosci. Model Dev., 4, 207–222, doi:10.5194/gmd-4-207-2011, 2011.

Bergamaschi, P., Frankenberg, C., Meirink, J. F., Krol, M., Villani, M. G., Houweling, S., Dentener, F., Dlugokencky, E. J., Miller, J. B., Gatti, L. V., Engel, A., and Levin, I.: Inverse modeling of global and regional CH_4 emissions using SCIAMACHY satellite retrievals, J. Geophys. Res., 114, D22301, doi:10.1029/2009JD012287, 2009.

Bergamaschi, P., Houweling, S., Segers, A., Krol, M., Frankenberg, C., Scheepmaker, R. A., Dlugokencky, E.,Wofsy, S. C., Kort, E. A., Sweeney, C., Schuck, T., Brenninkmeijer, C., Chen, H., Beck, V., and Gerbig, C.: Atmospheric CH_4 in the first decade of the 21st century: inverse modeling analysis using SCIAMACHY satellite retrievals and NOAA surface measurements, J. Geophys. Res., 118, 7350–7369, doi:10.1002/jgrd.50480, 2013.

Borsdorff, T. and Sussmann, R.: On seasonality of stratomesospheric CO above midlatitudes: New insight from solar FTIR spectrometry at Zugspitze and Garmisch, Geophys. Res. Lett., 36, L21804, doi:10.1029/2009GL040056, 2009.

Bousquet, P., Ciais, P., Miller, J. B., Dlugokencky, E. J., Hauglustaine, D. A., Prigent, C., Van der Werf, G. R., Peylin, P., Brunke, E. G., Carouge, C., Langenfels, R. L., Lathiere, J., Papa, F., Ramonet, M., Schmidt, M., Steele, L. P., Tyler, S. C., and White, J.: Contribution of anthropogenic and natural sources to atmospheric methane variability, Nature, 443, 439–443, 2006.

Bousquet, P., Ringeval, B., Pison, I., Dlugokencky, E. J., Brunke, E.-G., Carouge, C., Chevallier, F., Fortems-Cheiney, A., Frankenberg, C., Hauglustaine, D. A., Krummel, P. B., Langenfelds, R. L., Ramonet, M., Schmidt, M., Steele, L. P., Szopa, S., Yver, C., Viovy, N., and Ciais, P.: Source attribution of the changes in atmospheric methane for 2006–2008, Atmos. Chem. Phys., 11, 3689–3700, doi:10.5194/acp-11-3689-2011, 2011.

Butz, A., Guerlet, S., Hasekamp, O., Schepers, D., Galli, A., Aben, I., Frankenberg, C., Hartmann, J. M., Tran, H., Kuze, A., Keppel-Aleks, G., Toon, G., Wunch, D., Wennberg, P., Deutscher, N., Griffith, D., Macatangay, R., Messerschmidt, J., Notholt, J., and Warneke, T.: Toward accurate CO_2 and CH_4 observations from GOSAT, Geophys. Res. Lett., 38, L14812, doi:10.1029/2011GL047888, 2011.

Chevallier, F., Deutscher, N., Conway, C. J., Ciais, P., Ciattaglia, L., Dohe, S., Fröhlich, M., Gomez-Pelaez, A. J., Griffith, D., Hase, F., Haszpra, L., Krummel, P., Kyrö, E., Labuschagne, C., Langenfelds, R., Machida, T., Maignan, F., Matsueda, H., Morino, I.,

AMTD
7, 6743–6790, 2014

Notholt, J., Ramonet, M., Sawa, Y., Schmidt, M., Sherlock, V., Steele, P., Strong, K., Sussmann, R., Wennberg, P., Wofsy, S., Worthy, D., Wunch, D., and Zimnoch, M.: Global CO_2 surface fluxes inferred from surface air-sample measurements and from surface retrievals of the CO_2 total column, Geophys. Res. Lett., 38, L24810, doi:10.1029/2011GL049899, 2011.

Cicerone, R. J. and Oremland, R. S.: Biogeochemical aspects of atmospheric methane, Global Biogeochem. Cy., 2, 299–327, doi:10.1029/GB002i004p00299, 1988.

de Laat, A. T. J., Gloudemans, A. M. S., Schrijver, H., Aben, I., Nagahama, Y., Suzuki, K., Mahieu, E., Jones, N. B., Paton-Walsh, C., Deutscher, N. M., Griffith, D. W. T., De Mazière, M., Mittermeier, R. L., Fast, H., Notholt, J., Palm, M., Hawat, T., Blumenstock, T., Hase, F., Schneider, M., Rinsland, C., Dzhola, A. V., Grechko, E. I., Poberovskii, A. M., Makarova, M. V., Mellqvist, J., Strandberg, A., Sussmann, R., Borsdorff, T., and Rettinger, M.: Validation of five years (2003–2007) of SCIAMACHY CO total column measurements using ground-based spectrometer observations, Atmos. Meas. Tech., 3, 1457–1471, doi:10.5194/amt-3-1457-2010, 2010.

De Mazière, M., Vigouroux, C., Bernath, P. F., Baron, P., Blumenstock, T., Boone, C., Brogniez, C., Catoire, V., Coffey, M., Duchatelet, P., Griffith, D., Hannigan, J., Kasai, Y., Kramer, I., Jones, N., Mahieu, E., Manney, G. L., Piccolo, C., Randall, C., Robert, C., Senten, C., Strong, K., Taylor, J., Tétard, C., Walker, K. A., and Wood, S.: Validation of ACE-FTS v2.2 methane profiles from the upper troposphere to the lower mesosphere, Atmos. Chem. Phys., 8, 2421–2435, doi:10.5194/acp-8-2421-2008, 2008.

Dlugokencky, E. J., Nisbet E. G., Fisher R., and Lowry, D.: Global atmospheric methane: budget, changes and dangers, Philos. T. Roy Soc. A, 369, 2058–2072, doi:10.1098/rsta.2010.0341, 2011.

Dohe, S., Sherlock, V., Hase, F., Gisi, M., Robinson, J., Sepúlveda, E., Schneider, M., and Blumenstock, T.: A method to correct sampling ghosts in historic near-infrared Fourier transform spectrometer (FTS) measurements, Atmos. Meas. Tech., 6, 1981–1992, doi:10.5194/amt-6-1981-2013, 2013.

Fraser, A., Palmer, P. I., Feng, L., Boesch, H., Cogan, A., Parker, R., Dlugokencky, E. J., Fraser, P. J., Krummel, P. B., Langenfelds, R. L., O'Doherty, S., Prinn, R. G., Steele, L. P., van der Schoot, M., and Weiss, R. F.: Estimating regional methane surface fluxes: the relative importance of surface and GOSAT mole fraction measurements, Atmos. Chem. Phys., 13, 5697–5713, doi:10.5194/acp-13-5697-2013, 2013.

AMTD
7, 6743–6790, 2014

Garcia, R. R., Marsh, D. R., Kinnison, D. E., Boville, B. A., and Sassi, F.: Simulation of secular trends in the middle atmosphere, 1950–2003, J. Geophys. Res., 112, D09301, doi:10.1029/2006JD007485, 2007.

Geibel, M. C., Messerschmidt, J., Gerbig, C., Blumenstock, T., Chen, H., Hase, F., Kolle, O., Lavrič, J. V., Notholt, J., Palm, M., Rettinger, M., Schmidt, M., Sussmann, R., Warneke, T., and Feist, D. G.: Calibration of column-averaged CH_4 over European TCCON FTS sites with airborne in-situ measurements, Atmos. Chem. Phys., 12, 8763–8775, doi:10.5194/acp-12-8763-2012, 2012.

Hase, F., Hannigan, J. W., Coffey, M. T., Goldman, A., Höpfner, M., Jones, N. B., Rinsland, C. P., and Wood, S. W.: Intercomparison of retrieval codes used for the analysis of high-resolution, ground-based FTIR measurements, J. Quant. Spectrosc. Ra., 87, 25–52, 2004.

Houweling, S., van der Werf, G. R., Goldewijk, K. K., Roeckmann, T., and Aben, I.: Early anthropogenic CH_4 emissions and the variation of CH_4 and $^{13}CH_4$ over the last millennium, Global Biogeochem. Cy., 22, GB1002, doi:10.1029/2007GB002961, 2008.

Houweling, S., Aben, I., Breon, F.-M., Chevallier, F., Deutscher, N., Engelen, R., Gerbig, C., Griffith, D., Hungershoefer, K., Macatangay, R., Marshall, J., Notholt, J., Peters, W., and Serrar, S.: The importance of transport model uncertainties for the estimation of CO_2 sources and sinks using satellite measurements, Atmos. Chem. Phys., 10, 9981–9992, doi:10.5194/acp-10-9981-2010, 2010.

Houweling, S., Krol, M., Bergamaschi, P., Frankenberg, C., Dlugokencky, E. J., Morino, I., Notholt, J., Sherlock, V., Wunch, D., Beck, V., Gerbig, C., Chen, H., Kort, E. A., Röckmann, T., and Aben, I.: A multi-year methane inversion using SCIAMACHY, accounting for systematic errors using TCCON measurements, Atmos. Chem. Phys., 14, 3991–4012, doi:10.5194/acp-14-3991-2014, 2014.

Kirschke, S., Bousquet, P., Ciais, P., Saunois, M., Canadell, J. G., Dlugokencky, E. J., Bergamaschi, P., Bergmann, D., Blake, D. R., Bruhwiler, L., Cameron-Smith, P., Castaldi, S., Chevallier, F., Feng, L., Fraser, A., Heimann, M., Hodson, E. L., Houweling, S., Josse, B., Fraser, P. J., Krummel, P. B., Lamarque, J. F., Langenfelds, R. L., Le Quere, C., Naik, V., O'Doherty, S., Palmer, P. I., Pison, I., Plummer, D., Poulter, B., Prinn, R. G., Rigby, M., Ringeval, B., Santini, M., Schmidt, M., Shindell, D. T., Simpson, I., Spahni, R., Steele, L. P., Strode, S. A., Sudo, K., Szopa, S., van der Werf, G. R., Voulgarakis, A., van Weele, M., Weiss, R. F., Williams, J. E., and Zeng, G.: Three decades of global methane sources and sinks, Nat. Geosci., 6, 813–823, doi:10.1038/ngeo1955, 2013.

AMTD
7, 6743–6790, 2014

Kohlhepp, R., Ruhnke, R., Chipperfield, M. P., De Mazière, M., Notholt, J., Barthlott, S., Batchelor, R. L., Blatherwick, R. D., Blumenstock, Th., Coffey, M. T., Demoulin, P., Fast, H., Feng, W., Goldman, A., Griffith, D. W. T., Hamann, K., Hannigan, J. W., Hase, F., Jones, N. B., Kagawa, A., Kaiser, I., Kasai, Y., Kirner, O., Kouker, W., Lindenmaier, R., Mahieu, E., Mittermeier, R. L., Monge-Sanz, B., Morino, I., Murata, I., Nakajima, H., Palm, M., Paton-Walsh, C., Raffalski, U., Reddmann, Th., Rettinger, M., Rinsland, C. P., Rozanov, E., Schneider, M., Senten, C., Servais, C., Sinnhuber, B.-M., Smale, D., Strong, K., Sussmann, R., Taylor, J. R., Vanhaelewyn, G., Warneke, T., Whaley, C., Wiehle, M., and Wood, S. W.: Observed and simulated time evolution of HCl, $ClONO_2$, and HF total column abundances, Atmos. Chem. Phys., 12, 3527–3556, doi:10.5194/acp-12-3527-2012, 2012.

Lin, M., Fiore, A. M., Cooper, O. R., Horowitz, L. W., Langford, A. O., Levy II, H., Johnson, B. J., Naik, V., Oltmans, S. J., and Senff, C. J. : Springtime high surface ozone events over the western United States: quantifying the role of stratospheric intrusions, J. Geophys. Res., 117, D00V22, doi:10.1029/2012JD018151, 2012.

Lindenmaier, R., Strong, K., Batchelor, R. L., Chipperfield, M. P., Daffer, W. H., Drummond, J. R., Duck, T. J., Fast, H., Feng, W., Fogal, P. F., Kolonjari, F., Manney, G. L., Manson, A., Meek, C., Mittermeier, R. L., Nott, G. J., Perro, C., and Walker, K. A.: Unusually low ozone, HCl, and HNO_3 column measurements at Eureka, Canada during winter/spring 2011, Atmos. Chem. Phys., 12, 3821–3835, doi:10.5194/acp-12-3821-2012, 2012.

Messerschmidt, J., Geibel, M. C., Blumenstock, T., Chen, H., Deutscher, N. M., Engel, A., Feist, D. G., Gerbig, C., Gisi, M., Hase, F., Katrynski, K., Kolle, O., Lavrič, J. V., Notholt, J., Palm, M., Ramonet, M., Rettinger, M., Schmidt, M., Sussmann, R., Toon, G. C., Truong, F., Warneke, T., Wennberg, P. O., Wunch, D., and Xueref-Remy, I.: Calibration of TCCON column-averaged CO_2: the first aircraft campaign over European TCCON sites, Atmos. Chem. Phys., 11, 10765–10777, doi:10.5194/acp-11-10765-2011, 2011.

Monteil, G., Houweling, S., Butz, A., Guerlet, S., Schepers, D., Hasekamp, O., Frankenberg, C., Scheepmaker, R., Aben, I., and Röckmann, T.: Comparison of CH_4 inversions based on 15 months of GOSAT and SCIAMACHY observations, J. Geophys. Res.-Atmos., 118, 11807–11823, doi:10.1002/2013JD019760, 2013.

Morino, I., Uchino, O., Inoue, M., Yoshida, Y., Yokota, T., Wennberg, P. O., Toon, G. C., Wunch, D., Roehl, C. M., Notholt, J., Warneke, T., Messerschmidt, J., Griffith, D. W. T., Deutscher, N. M., Sherlock, V., Connor, B., Robinson, J., Sussmann, R., and Rettinger, M.: Preliminary validation of column-averaged volume mixing ratios of carbon dioxide and

AMTD
7, 6743–6790, 2014

methane retrieved from GOSAT short-wavelength infrared spectra, Atmos. Meas. Tech., 4, 1061–1076, doi:10.5194/amt-4-1061-2011, 2011.

Nash, E. R., Newman, P. A., Rosenfield, J. E., and Schoeberl, M. R.: An objective determination of the polar vortex using Ertel's potential vorticity, J. Geophys. Res., 101, 9471–9478, 1996.

Patra, P. K., Takigawa, M., Ishijima, K., Choi, B.-C., Cunnold, D., Dlugokencky, E. J., Fraser, P., Gomez-Pelaez, A. J., Goo, T.-Y., Kim, J. S., Krummel, P., Langenfelds, R., Meinhardt, F., Mukai, H., O'Doherty, S., Prinn, R. G., Simmonds, P., Steele, P., Tohjima, Y., Tsuboi, K., Uhse, K., Weiss, R., Worthy, D., and Nakazawa, T. : Growth rate, seasonal, synoptic, diurnal variations and budget of methane in lower atmosphere, J. Meteorol. Soc. Jpn., 87, 635–663, 2009.

Patra, P. K., Houweling, S., Krol, M., Bousquet, P., Belikov, D., Bergmann, D., Bian, H., Cameron-Smith, P., Chipperfield, M. P., Corbin, K., Fortems-Cheiney, A., Fraser, A., Gloor, E., Hess, P., Ito, A., Kawa, S. R., Law, R. M., Loh, Z., Maksyutov, S., Meng, L., Palmer, P. I., Prinn, R. G., Rigby, M., Saito, R., and Wilson, C.: TransCom model simulations of CH_4 and related species: linking transport, surface flux and chemical loss with CH_4 variability in the troposphere and lower stratosphere, Atmos. Chem. Phys., 11, 12813–12837, doi:10.5194/acp-11-12813-2011, 2011.

Pougatchev, N. S., Connor, B. J., and Rinsland, C. P.: Infrared measurements of the ozone vertical distribution above Kitt Peak, J. Geophys. Res., 100, 16689–16697, 1995.

Rodgers, C. D.: Inverse Methods for Atmospheric Sounding: Theory and Practice, Vol. 2 of Series on Atmospheric, Oceanic and Planetary Physics, edited by: Taylor, F. W., World Scientific, 2000.

Saito, R., Patra, P. K., Deutscher, N., Wunch, D., Ishijima, K., Sherlock, V., Blumenstock, T., Dohe, S., Griffith, D., Hase, F., Heikkinen, P., Kyrö, E., Macatangay, R., Mendonca, J., Messerschmidt, J., Morino, I., Notholt, J., Rettinger, M., Strong, K., Sussmann, R., and Warneke, T.: Technical Note: Latitude-time variations of atmospheric column-average dry air mole fractions of CO_2, CH_4 and N_2O, Atmos. Chem. Phys., 12, 7767–7777, doi:10.5194/acp-12-7767-2012, 2012.

Sapart, S. J., Monteil, G., Prokopiou, M., van de Wal, R. S. W., Kaplan, J. O., Sperlich, P., Krumhardt, K. M., van der Veen, C., Houweling, S., Krol, M. C., Blunier, T., Sowers, T., Martinerie, P., Witrant, E., Dahl-Jensen, D., and Röckmann, T.: Natural and anthropogenic variations in methane sources during the past two millennia, Nature, 490, 85–88, doi:10.1038/nature11461, 2012.

AMTD
7, 6743–6790, 2014

Schneising, O., Bergamaschi, P., Bovensmann, H., Buchwitz, M., Burrows, J. P., Deutscher, N. M., Griffith, D. W. T., Heymann, J., Macatangay, R., Messerschmidt, J., Notholt, J., Rettinger, M., Reuter, M., Sussmann, R., Velazco, V. A., Warneke, T., Wennberg, P. O., and Wunch, D.: Atmospheric greenhouse gases retrieved from SCIAMACHY: comparison to ground-based FTS measurements and model results, Atmos. Chem. Phys., 12, 1527–1540, doi:10.5194/acp-12-1527-2012, 2012.

Sepúlveda, E., Schneider, M., Hase, F., García, O. E., Gomez-Pelaez, A., Dohe, S., Blumenstock, T., and Guerra, J. C.: Long-term validation of tropospheric column-averaged CH_4 mole fractions obtained by mid-infrared ground-based FTIR spectrometry, Atmos. Meas. Tech., 5, 1425–1441, doi:10.5194/amt-5-1425-2012, 2012.

Sinnhuber, B.-M., Stiller, G., Ruhnke, R., von Clarmann, T., Kellmann, S., and Aschmann, J.:, Arctic winter 2010/2011 at the brink of an ozone hole, Geophys. Res. Lett., 38, L24814, doi:10.1029/2011GL049784, 2011.

Sprenger, M. and Wernli, H.: A northern hemispheric climatology of crosstropopause exchange for the ERA15 time period (1979–1993), J. Geophys. Res., 108, 8521, doi:10.1029/2002JD002636, 2003.

Stocker, T., Qin, D., Plattner, G. K., Tignor, M., Allen, S. K., Boschung, J., Nauels, A., Xia, Y., Bex, V., and Midgley, P. M. (Eds.): Summary for Policymakers, Climate Change 2013: The Physical Science Basis. Contribution of Working Group I to the Fifth Assessment Report of the Intergovernmental Panel on Climate Change, Cambridge University Press, Cambridge, United Kingdom and New York, NY, USA, 2013.

Stohl, A. and Trickl, T.: A textbook example of long-range transport: Simultaneous observation of ozone maxima of stratospheric and North American origin in the free troposphere over Europe, J. Geophys. Res., 104, 30445–30462, 1999.

Stohl, A., Spichtinger-Rakowsky, N., Bonasoni, P., Feldmann, H., Memmesheimer, M., Scheel, H. E., Trickl, T., Hübener, S. H., Ringer, W., and Mandl, M.: The influence of stratospheric intrusions on alpine ozone concentrations, Atmos. Environ., 34, 1323–1354, 2000.

Stohl, A., Bonasoni, P., Cristofanelli, P., Collins, W., Feichter, J., Frank, A., Forster, C., Gerasopoulos, E., Gäggeler, H., James, P., Kentarchos, T., Kromp-Kolb, H., Krüger, B., Land, C., Meloen, J., Papayannis, A., Priller, A., Seibert, P., Sprenger, M., Roelofs, G. J., Scheel, H. E., Schnabel, C., Siegmund, P., Tobler, L., Trickl, T., Wernli, H., Wirth, V., Zanis, P., and Zerefos, C.: Stratosphere-troposphere exchange: a review, and what we have learned from STACCATO, J. Geophys. Res., 108, 8516, doi:10.1029/2002JD002490, 2003.

AMTD
7, 6743–6790, 2014

Sussmann, R., Stremme, W., Buchwitz, M., and de Beek, R.: Validation of ENVISAT/SCIAMACHY columnar methane by solar FTIR spectrometry at the Ground-Truthing Station Zugspitze, Atmos. Chem. Phys., 5, 2419–2429, doi:10.5194/acp-5-2419-2005, 2005.

Sussmann, R., Borsdorff, T., Rettinger, M., Camy-Peyret, C., Demoulin, P., Duchatelet, P., Mahieu, E., and Servais, C.: Technical Note: Harmonized retrieval of column-integrated atmospheric water vapor from the FTIR network – first examples for long-term records and station trends, Atmos. Chem. Phys., 9, 8987–8999, doi:10.5194/acp-9-8987-2009, 2009.

Sussmann, R., Forster, F., Rettinger, M., and Jones, N.: Strategy for high-accuracy-and-precision retrieval of atmospheric methane from the mid-infrared FTIR network, Atmos. Meas. Tech., 4, 1943–1964, doi:10.5194/amt-4-1943-2011, 2011.

Sussmann, R., Forster, F., Rettinger, M., and Bousquet, P.: Renewed methane increase for five years (2007–2011) observed by solar FTIR spectrometry, Atmos. Chem. Phys., 12, 4885–4891, doi:10.5194/acp-12-4885-2012, 2012.

Sussmann, R., Ostler, A., Forster, F., Rettinger, M., Deutscher, N. M., Griffith, D. W. T., Hannigan, J. W., Jones, N., and Patra, P. K.: First intercalibration of column-averaged methane from the Total Carbon Column Observing Network and the Network for the Detection of Atmospheric Composition Change, Atmos. Meas. Tech., 6, 397–418, doi:10.5194/amt-6-397-2013, 2013.

Toon, G. C., Farmer, C. B., Schaper, P. W., Lowes, L. L., Norton, R. H., Schoeberl, M. R., Lait, L. R., and Newman, P. A.: Evidence for subsidence in the 1989 Polar winter stratosphere from airborne infrared composition measurements, J. Geophys. Res., 97, 7963–7970, 1992.

Trickl, T., Cooper, O. C., Eisele, H., James, P., Mücke, R., and Stohl, A.: Intercontinental transport and its influence on the ozone concentrations over central Europe: three case studies, J. Geophys. Res., 108, 8530, doi:10.1029/2002JD002735, 2003.

Trickl, T., Feldmann, H., Kanter, H.-J., Scheel, H.-E., Sprenger, M., Stohl, A., and Wernli, H.: Forecasted deep stratospheric intrusions over Central Europe: case studies and climatologies, Atmos. Chem. Phys., 10, 499–524, doi:10.5194/acp-10-499-2010, 2010.

Trickl, T., Vogelmann H., Giehl H., Scheel H.-E., Sprenger M., and Stohl A.: How stratospheric are deep stratospheric intrusions? Part 1: Lidar measurements of ozone and water vapour, in preparation, 2014.

Wernli, H. and Davies, H. C.: A Lagrangian-based analysis of extratropical cyclones, I, The method and some applications, Q. J. Roy. Meteorol. Soc., 123, 467– 489, 1997.

AMTD
7, 6743–6790, 2014

Wofsy, S. C. and the HIPPO Science Team and Cooperating Modellers and Satellite Teams: TS6 HIAPER Pole-to-Pole Observations (HIPPO): fine-grained, global-scale measurements of climatically important atmospheric gases and aerosols, Philos. T. Roy. Soc. A, 369, 2073–2086, 2011.

Wunch, D., Toon, G. C., Wennberg, P. O., Wofsy, S. C., Stephens, B. B., Fischer, M. L., Uchino, O., Abshire, J. B., Bernath, P., Biraud, S. C., Blavier, J.-F. L., Boone, C., Bowman, K. P., Browell, E. V., Campos, T., Connor, B. J., Daube, B. C., Deutscher, N. M., Diao, M., Elkins, J. W., Gerbig, C., Gottlieb, E., Griffith, D. W. T., Hurst, D. F., Jiménez, R., Keppel-Aleks, G., Kort, E. A., Macatangay, R., Machida, T., Matsueda, H., Moore, F., Morino, I., Park, S., Robinson, J., Roehl, C. M., Sawa, Y., Sherlock, V., Sweeney, C., Tanaka, T., and Zondlo, M. A.: Calibration of the Total Carbon Column Observing Network using aircraft profile data, Atmos. Meas. Tech., 3, 1351–1362, doi:10.5194/amt-3-1351-2010, 2010.

Wunch, D., Toon, G. C., Blavier, J.-F. L., Washenfelder, R. A., Notholt, J., Connor, B. J., Griffith, D. W. T., Sherlock, V., and Wennberg, P. O.: The total carbon column observing network, Philos. T. Roy Soc. A, 369, 2087–2112, doi:10.1098/rsta.2010.0240, 2011a.

Wunch, D., Wennberg, P. O., Toon, G. C., Connor, B. J., Fisher, B., Osterman, G. B., Frankenberg, C., Mandrake, L., O'Dell, C., Ahonen, P., Biraud, S. C., Castano, R., Cressie, N., Crisp, D., Deutscher, N. M., Eldering, A., Fisher, M. L., Griffith, D. W. T., Gunson, M., Heikkinen, P., Keppel-Aleks, G., Kyrö, E., Lindenmaier, R., Macatangay, R., Mendonca, J., Messerschmidt, J., Miller, C. E., Morino, I., Notholt, J., Oyafuso, F. A., Rettinger, M., Robinson, J., Roehl, C. M., Salawitch, R. J., Sherlock, V., Strong, K., Sussmann, R., Tanaka, T., Thompson, D. R., Uchino, O., Warneke, T., and Wofsy, S. C.: A method for evaluating bias in global measurements of CO_2 total columns from space, Atmos. Chem. Phys., 11, 12317–12337, doi:10.5194/acp-11-12317-2011, 2011b.

Xiong, X., Barnet, C., Maddy, E., Wofsy, S. C., Chen, L., Karion, A., and Sweeney, C.: Detection of methane depletion associated with stratospheric intrusion by atmospheric infrared sounder (AIRS), Geophys. Res. Lett., 40, 2455–2459, doi:10.1002/grl.50476, 2013.

Yoshida, Y., Ota, Y., Eguchi, N., Kikuchi, N., Nobuta, K., Tran, H., Morino, I., and Yokota, T.: Retrieval algorithm for CO_2 and CH_4 column abundances from short-wavelength infrared spectral observations by the Greenhouse gases observing satellite, Atmos. Meas. Tech., 4, 717–734, doi:10.5194/amt-4-717-2011, 2011.

AMTD
7, 6743–6790, 2014

Table 1. The FTIR stations of this NDACC versus TCCON intercomparison of XCH_4 along with geographical coordinates and the time period of FTIR measurements used.

Site	Latitude	Longitude	Altitude	Time period
Garmisch	47.48° N	11.06° E	0.743 km	Jul 2007–Dec 2012
Wollongong	34.41° S	150.88° E	0.030 km	Jun 2008–Dec 2012
Izaña	28.31° N	16.45° W	2.370 km	Dec 2010–Dec 2012
Karlsruhe	49.08° N	8.43° E	0.110 km	Apr 2010–Dec 2012
Ny-Ålesund	78.92° N	11.93° E	0.020 km	Mar 2005–Aug 2012

AMTD
7, 6743–6790, 2014

Table 2. Intercept and slope of linear scatter plot fits between multi-annual data sets of NIR and MIR XCH_4 retrievals using varied a priori profiles. Data are monthly means constructed from same-day measurement coincidences.

		fit $y = bx$		
data set	a priori	slope b and 2-σ uncertainty	slope different from 1 on 2-σ level?	stdv(ppb)
Garmisch	NIR & MIR retrieved with original a priori	1.0002(12)	no	8.6
	NIR & MIR corrected to ACTM a priori	0.9994(09)	no	6.3
Wollongong	NIR & MIR retrieved with original a priori	1.0010(13)	no	7.4
	NIR & MIR corrected to ACTM a priori	1.0030(11)	yes	6.1
Izaña	NIR & MIR retrieved with original a priori	0.9986(06)	yes	2.5
	NIR & MIR corrected to ACTM a priori	1.0007(07)	no	3.0
Karlsruhe	NIR & MIR retrieved with original a priori	0.9996(13)	no	6.1
	NIR & MIR corrected to ACTM a priori	1.0024(11)	yes	5.1
Ny-Ålesund	NIR & MIR retrieved with original a priori	0.9909(22)	yes	13.0
	NIR & MIR corrected to ACTM a priori	0.9940(19)	yes	11.5

AMTD
7, 6743–6790, 2014

Table 3. As Table 2, but only for Ny-Ålesund. The data set "Ny-Ålesund PV-filter" corresponds to MIR and NIR retrievals that are not influenced by the polar vortex.

		fit $y = bx$		
data set	a priori	slope b and 2-σ uncertainty	slope different from 1 on 2-σ level?	stdv(ppb)
Ny-Ålesund	NIR & MIR retrieved with original a priori	0.9909(22)	yes	13.0
Ny-Ålesund PV-filter	NIR & MIR retrieved with original a priori	0.9922(23)	yes	12.4
Ny-Ålesund	NIR & MIR corrected to ACTM a priori	0.9940(19)	yes	11.5
Ny-Ålesund PV-filter	NIR & MIR corrected to ACTM a priori	0.9950(20)	yes	11.0

AMTD
7, 6743–6790, 2014

Table 4. As Table 2, but only for Garmisch using MIR and NIR retrievals which are coincident to the STE trajectory data set. Data sets are divided into monthly means using measurements from all days ("Garmisch complete") or only days without STE-events at Garmisch ("Garmisch without STE").

		fit $y = bx$		
data set	a priori	slope b and 2-σ uncertainty	slope different from 1 on 2-σ level?	stdv(ppb)
Garmisch complete	NIR & MIR retrieved with original a priori	1.0001(12)	no	8.2
Garmisch without STE	NIR & MIR retrieved with original a priori	1.0015(11)	yes	6.5
Garmisch complete	NIR & MIR corrected to ACTM a priori	0.9993(09)	no	6.2
Garmisch without STE	NIR & MIR corrected to ACTM a priori	1.0002(08)	no	4.7

AMTD
7, 6743–6790, 2014

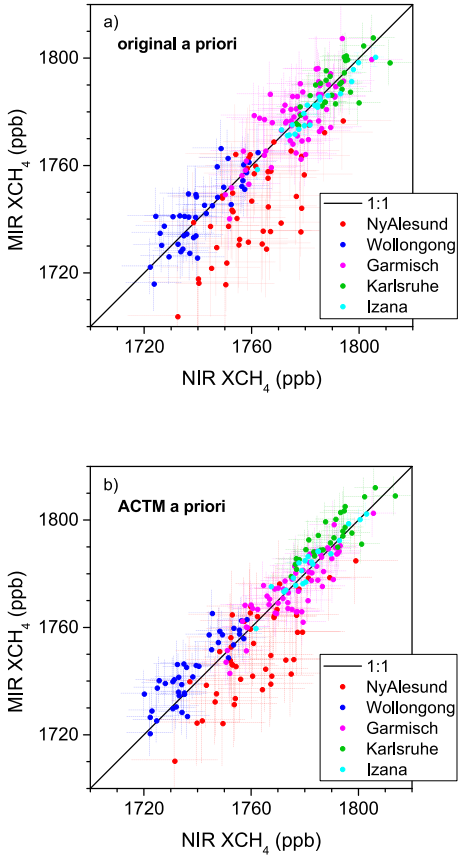

Figure 1. (a) Scatter plot of MIR and NIR monthly means, both series retrieved with the standard retrieval a priori profiles. Error bars on data points are 2σ uncertainties derived from the stdv of the linear slope fit ($2\,\mathrm{stdv}/\sqrt{2}$). **(b)** Same as **(a)** but for using ACTM profiles as common prior.

AMTD
7, 6743–6790, 2014

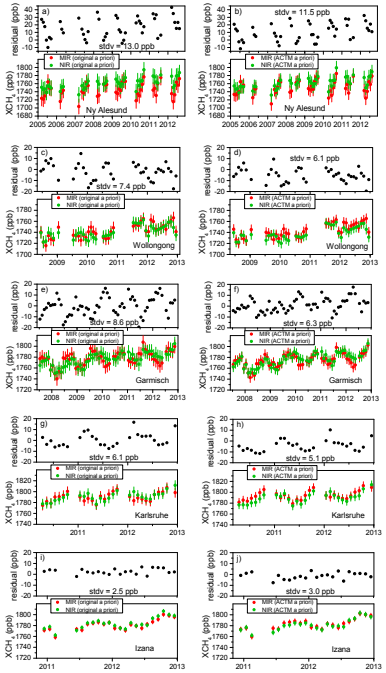

Figure 2. (a) Lower trace: monthly-mean MIR and NIR time series for Ny-Ålesund. Both column series are plotted as retrieved with their original retrieval a priori profiles. Error bars are 2-σ uncertainites as explained in Fig. 1. Upper trace: Residual time series, i.e. difference time series of the NIR and MIR data shown in the lower trace. **(b)** Same as **(a)** but using for Ny-Ålesund a correction to 3 hourly ACTM profiles as common prior, **(c)** for Wollongong the original retrieval a priori profiles, **(d)** for Wollongong a correction to ACTM, **(e)** for Garmisch the original retrieval a priori profiles, **(f)** for Garmisch a correction to ACTM, **(g)** for Karlsruhe the original retrieval a priori profiles, **(h)** for Garmisch a correction to ACTM, **(i)** for Izaña the original retrieval a priori profiles, and **(j)** for Izaña a correction to ACTM.

AMTD
7, 6743–6790, 2014

Multi-station intercomparison of column-averaged methane

A. Ostler et al.

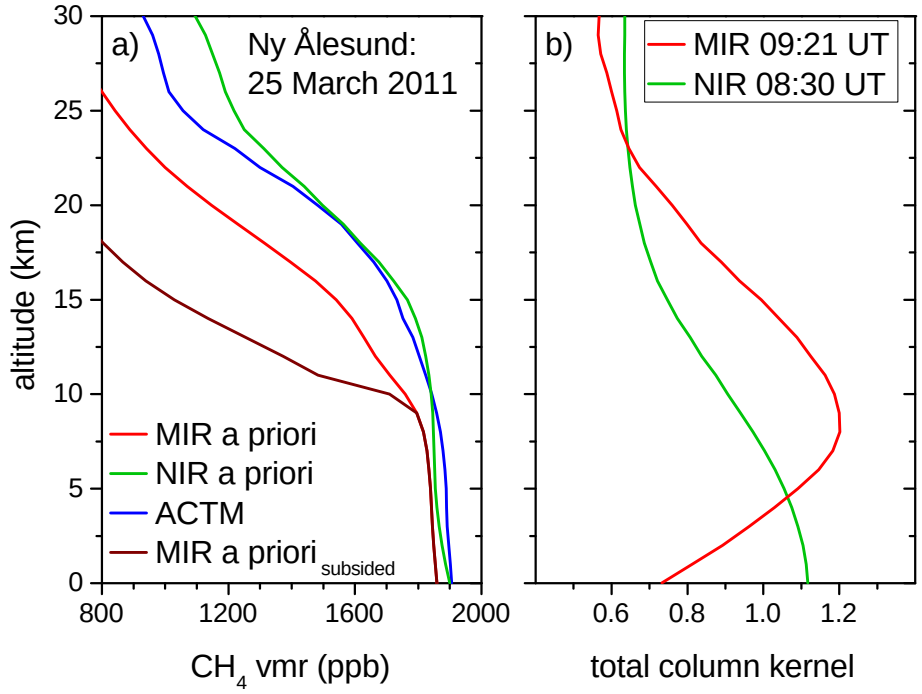

Figure 3. (a) A priori profiles used for analysis of Ny-Ålesund spectra recorded on 25 March 2011. MIR a priori is the standard a priori profile from WACCM for Ny-Ålesund used in SFIT. NIR a priori is the current a priori profile of GFIT (release ggg_2012_July_Update) for Ny-Ålesund. ACTM is the actual ACTM profile for 25 March 2011 used as a common prior for standard intercomparison of the NIR and MIR retrievals. MIR a priori$_{subsided}$ is a strongly subsided profile typical for intra-vortex conditions as explained in Appendix B used for re-correction of the NIR and MIR retrievals in a more realistic intercomparison. **(b)** Averaging kernels for MIR and NIR retrievals of Ny-Ålesund spectra recorded on 25 March 2011.

AMTD
7, 6743–6790, 2014

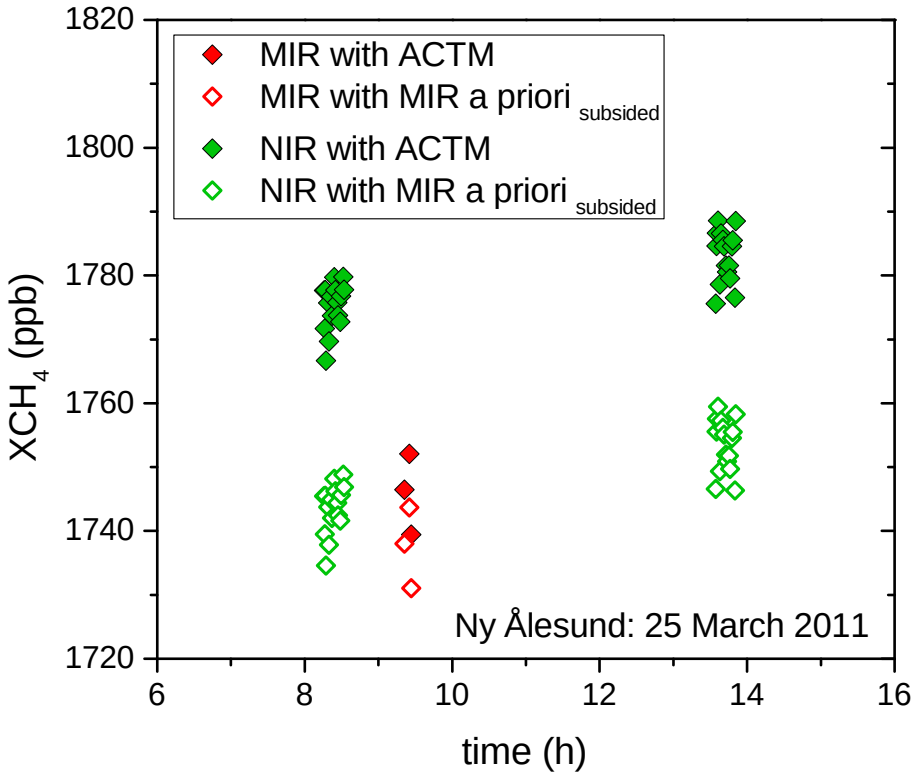

Figure 4. Ny-Ålesund XCH_4 on 25 March 2011 retrieved from FTIR data. MIR and NIR retrievals are corrected to the common ACTM prior (filled squares) and are corrected to a strongly subsided MIR a priori profile (open squares) as shown in Fig. 3a.

AMTD
7, 6743–6790, 2014

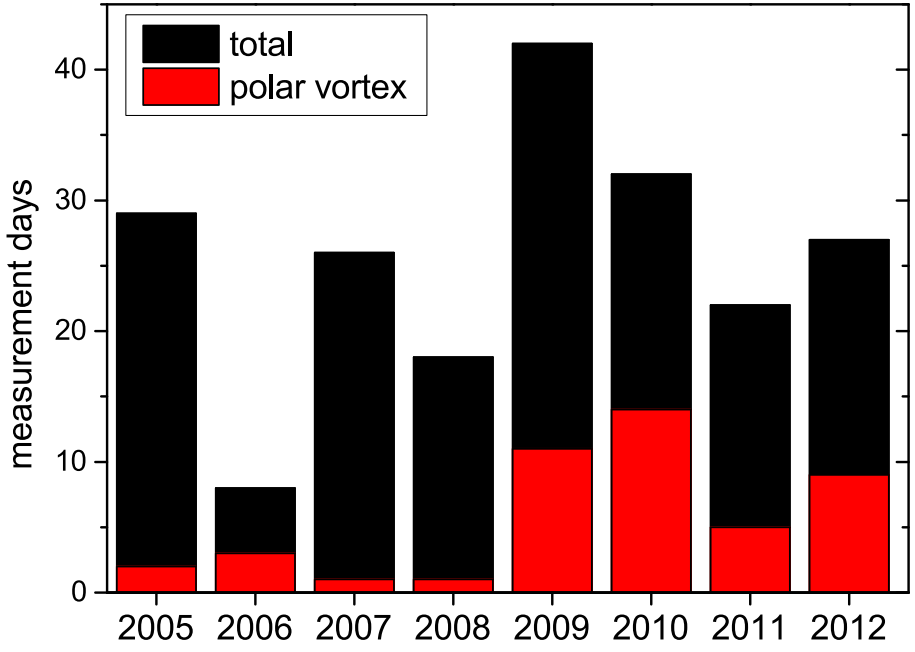

Figure 5. Number of days with coincident MIR and NIR FTIR measurements at Ny-Ålesund. Black: total number, red: only measurement days when the station has been inside the polar vortex.

AMTD
7, 6743–6790, 2014

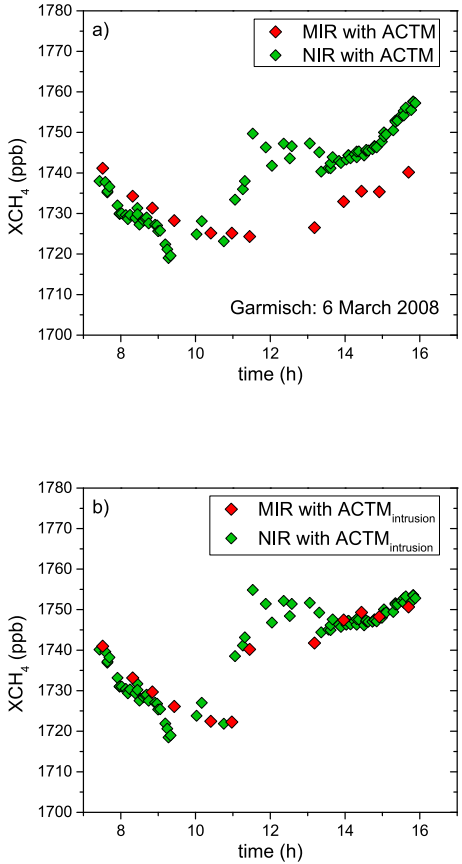

Figure 6. Garmisch XCH_4 on 6 March 2008 retrieved from FTIR data. **(a)** MIR and NIR retrievals are corrected to a common ACTM a priori. **(b)** MIR and NIR retrievals are corrected to the modified ACTM profiles shown in Fig. 10a.

AMTD
7, 6743–6790, 2014

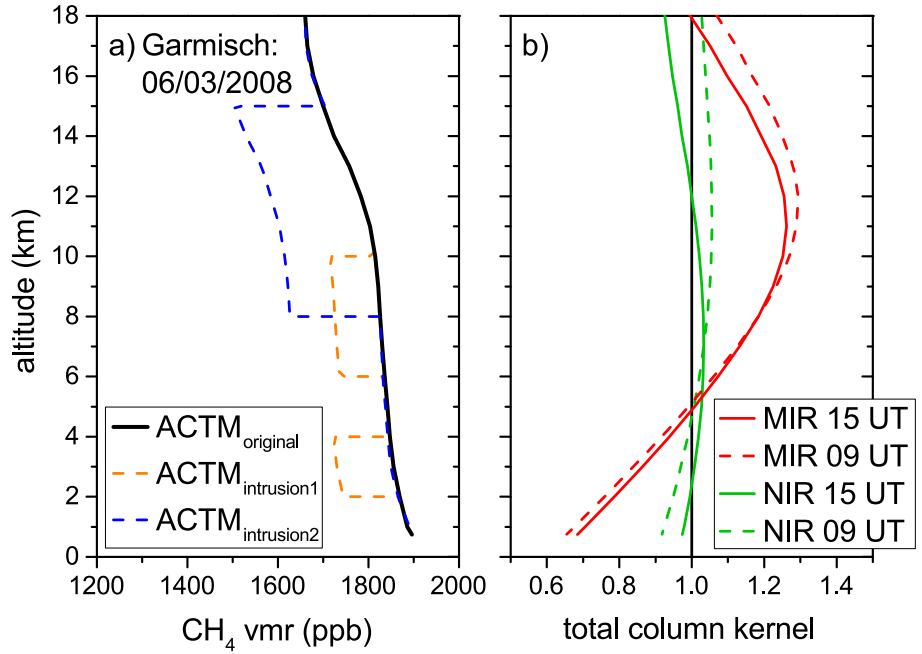

Figure 7. (a) ACTM profiles used for the a posteriori correction of MIR and NIR retrievals of Garmisch spectra recorded on 6 March 2008: $ACTM_{original}$ is the original ACTM profile used in the correction. $ACTM_{intrusion1}$ and $ACTM_{intrusion2}$ are the original ACTM profiles which were modified due to a deep stratospheric intrusion event on this day. $ACTM_{intrusion1}$ is used for the re-correction of retrievals before 11:00 UTC, $ACTM_{intrusion2}$ is used for the re-correction of retrievals after 11:00 UTC. **(b)** Averaging kernels for MIR and NIR retrievals of Garmisch spectra recorded on 6 March 2008.

AMTD
7, 6743–6790, 2014

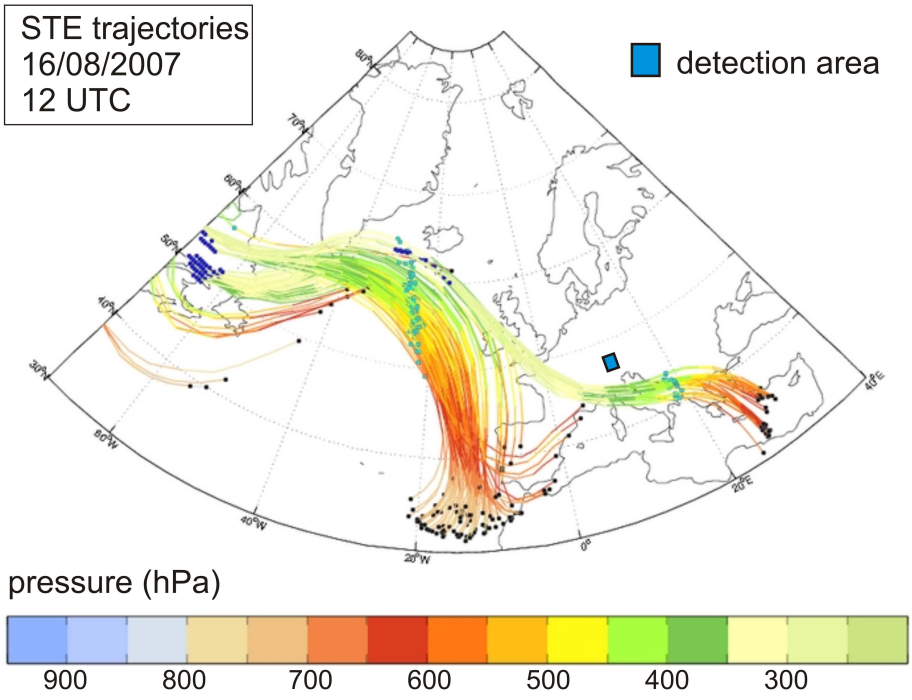

Figure 8. STE trajectories calculated with the tool of ETH Zürich, based on ECMWF data. The trajectories were initiated on 16 August 2007 at t_0 = 12:00 UTC. The time positions on the trajectories for t_0, $t_0 + 2$ d and $t_0 + 4$ d are marked by azur, cyan, and black dots, respectively. The frame of the detection area (2° × 2°) around Garmisch is marked by the blue square.

AMTD
7, 6743–6790, 2014

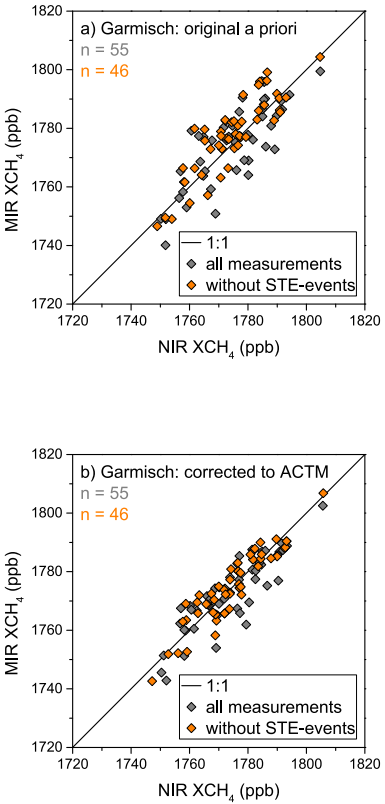

Figure 9. Scatter plot of MIR and NIR monthly means for Garmisch XCH_4 obtained from all FTIR measurements (black diamonds) and FTIR measurements which are not affected by STE-events (red diamonds), respectively. **(a)** MIR and NIR XCH_4 retrieved with their original retrieval a priori profiles and **(b)** a posteriori corrected to common ACTM profiles. Note: data set is not identical to Sect. 3 because STE trajectories are not available for the complete time series.

AMTD
7, 6743–6790, 2014

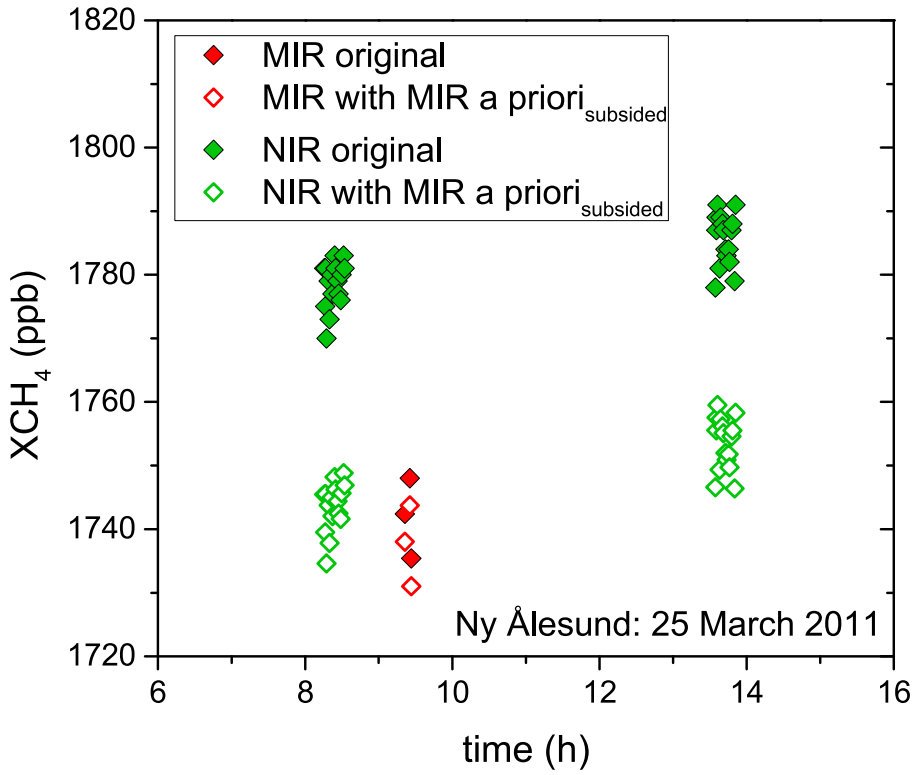

Figure C1. Same as Fig. 4 but MIR and NIR retrievals as computed with their standard (original) retrieval a priori (filled squares) and as corrected to a strongly subsided MIR a priori profile (open squares) as shown in Fig. 3a.

AMTD
7, 6743–6790, 2014

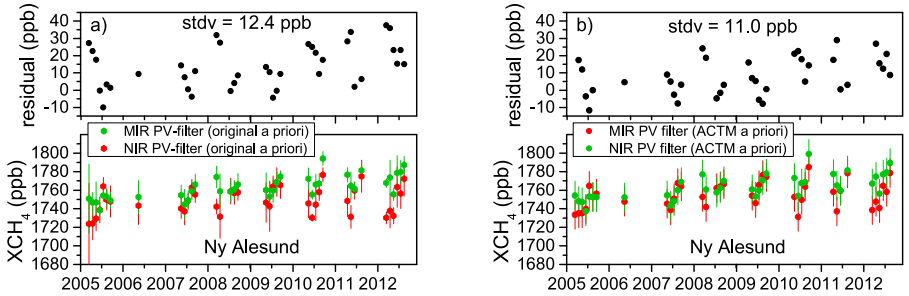

Figure C2. Same as Fig. 2 for Ny-Ålesund but excluding retrievals affected from stratospheric subsidence via PV as an extra filter criterion (see Sect. 4.1.2). **(a)** NIR and MIR retrievals with their original standard retrieval a priori. **(b)** NIR and MIR retrievals corrected to the common ACTM priori.

AMTD
7, 6743–6790, 2014

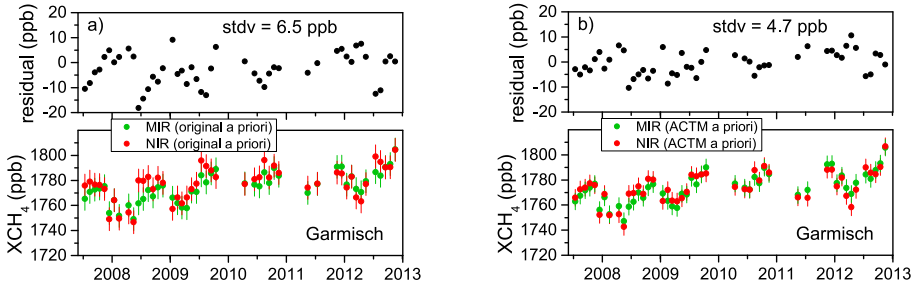

Figure C3. Same as Fig. 2 for Garmisch but excluding retrievals affected from STE-events (see Sect. 4.2.2). **(a)** NIR and MIR retrievals with their original standard retrieval a priori. **(b)** NIR and MIR retrievals corrected to the common ACTM priori.

AMTD
7, 6743–6790, 2014